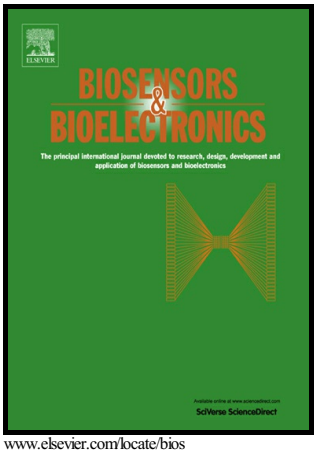

www.elsevier.com/locate/bios

Liquid crystal-based biosensor with backscattering interferometry: a quantitative approach

Mashooq Khan, Soo-Young Park

PII: S0956-5663(16)30949-6
DOI: http://dx.doi.org/10.1016/j.bios.2016.09.065
Reference: BIOS9177

To appear in: *Biosensors and Bioelectronic*

Received date: 3 July 2016
Revised date: 11 September 2016
Accepted date: 19 September 2016

Cite this article as: Mashooq Khan and Soo-Young Park, Liquid crystal-base biosensor with backscattering interferometry: a quantitative approach, *Biosensor and Bioelectronic,* http://dx.doi.org/10.1016/j.bios.2016.09.065

Liquid crystal-based biosensor with backscattering interferometry: a quantitative approach

Mashooq Khan, Soo-Young Park*

Department of Polymer Science & Engineering, Polymeric Nanomaterials Laboratory, School of Applied Chemical Engineering, Kyungpook National University, #1370 Sangyuk-dong, Buk-gu, Daegu 41566, Korea

*Corresponding author: psy@knu.ac.kr

Abstract

We developed a new technology that uses backscattering interferometry (BSI) to quantitatively measure nematic liquid crystal (NLC)-based biosensors, which usually had relied on texture reading for on/off signals. The LC-based BSI comprised an octadecyltrichlorosilane (OTS)-coated square capillary filled with 4-cyano-4′-pentylbiphenyl (5CB, a nematic LC at room temperature). The LC/water interface in the capillary was functionalized by a coating of poly(acrylicacid-b-4-cyanobiphenyl-4′-undecylacrylate) (PAA-b-LCP) and immobilized with the enzymes glucose oxidase (GOx) and horseradish peroxidase (HRP) through covalent linkage to the PAA chains ($5CB_{PAA\text{-}GOx:HRP}$) for glucose detection. Laser irradiation of the LC near the LC/water interface resulted in backscattered fringes with high contrast. The change in the spatial position of the fringes (because of the change in the orientation of the LC caused by the GOx:HRP enzymatic reaction of glucose) altered the output voltage of the photodetector when its active area was aligned with the edge of one of the fringes. The change in the intensity at the photodetector allowed the detection limit of the instrument to be as low as 0.008mM with a

linear range of 0.02–9 mM in a short response time (~60 s). This LC-based BSI technique allows for quantitative, sensitive, selective, reproducible, easily obtainable, and interference-free detection in a large linear dynamic range and for practical applications with human serum.

Keywords: Laser interferometer, liquid crystal, biosensor, glucose, fringe

1. Introduction:

Over the last twenty years, nematic liquid crystals (NLC) have received considerable attention with respect to the development of biosensors. The high sensitivity of NLC orientation to external stimuli, the long-range order, and high optical anisotropy of LC molecules can transform chemical and biomolecular binding events into amplified optical signals. LC-based detection can be performed in ambient light without electrical power or molecular labels, and the optical output of the NLCs can be easily observed using a polarized optical microscope (POM). Because of these superior properties, there have been efforts to develop LC-based biosensors for the detection of proteins,(Gupta et al. 1998) lipids,(Brake et al. 2003; Lin et al. 2011; Symietz et al. 2004; Zhao et al. 2006) nucleic acid hybridization,(Chen et al. 1998; Tan et al. 2010) glucose,(Khan and Park 2014b, 2015b; Kim et al. 2013) urea,(Khan et al. 2014; Khan and Park 2014a) cholic acid,(Deng et al. 2016; Niu et al. 2016) cholesterol,(Munir and Park 2015; Tyagi et al. 2014; Zhao et al. 2015), histidine,(Liao et al. 2016), myricetin,(Munir and Park 2016) and pathogens.(Khan et al. 2016) However, LC-based biosensors have been used mainly for qualitative observation of optical texture but rarely for quantitative measurement.

Some optical properties of LCs are reflection, refraction, optical absorption, optical activity, harmonic generation, optical wave guidance, light scattering, and response to high-frequency electromagnetic radiation.(Hsu et al. 1998; Malik and Raina 2004) These properties are described in terms of optical anisotropy, which arises from the distinct refractive indices measured parallel ($n_{\parallel}$) and perpendicular ($n_{\perp}$) to the local nematic director ($\vec{n}$).(Loudet et al. 2004)When a light beam propagates at an angle φrelative to the optical axis of the LC molecules, it splits into ordinary and extraordinary rays with refractive indices n_o and n_e, respectively. The difference between n_o and n_e is the optical birefringence (Δn), which is related to $n_{\parallel}$ and $n_{\perp}$ via φ, as seen in Eq.(1).

$$\Delta n = n_e - n_o = \frac{n_{\parallel} n_{\perp}}{\sqrt{n_{\parallel}^2 \cos\varphi + n_{\perp}^2 \sin^2\varphi}} - n_{\perp} \quad (1)$$

Ordinary and extraordinary beams propagate through an LC at different speeds, which causes a phase difference (Γ) and Δn (= Γ/d) within the LC molecules, where d is the optical distance that light of wavelength λ propagates in a vacuum. The molecules on the surface of an LC can have homeotropic or planar orientation or be at an angle to the surface.(Patel and Yokoyama 1993) In addition, the change in the orientation of the LC molecules near the surface can propagate to the LC mesogens up to 10^5 times the molecular length from the surface.(Carlton et al. 2012b) The planar orientation has a high Δn when the surface is observed perpendicularly because of the parallel orientation of the LC mesogens.(Carlton et al. 2012a; Khan and Park 2014b) The texture (color) of an LC observed by a polarized optical microscope (POM) under a crossed polarizer represents Δn,(Dierking 2003) which is strongly dependent on the tilt angle of the director with the surface normal.(Carlton et al. 2012a; Carlton et al. 2012b; Khan and Park

2015b)However, difficulty in measuring small changes in Δn in selected regions and a small linear dynamic range make this method unsuitable for quantitative detection and do not represent the whole area.

Light interferometry has been used as a laboratory technique for almost 100 years. However, several new developments such as the invention of the laser and increased use of photodetectors have extended the scope and accuracy of light interferometry. Lasers have removed many of the limitations imposed by conventional light sources, leading to many new applications for interferometry, including measurement of distance, displacement, vibration, temperature, pressure, electrical and magnetic fields, rotation sensing, and frequency; optical systems testing, studies of gas flow, plasmas, and surface topography; and high-resolution spectroscopy.(Hariharan 2007; Ready) Bornhop et al.(Bornhop et al. 2007; Haddad et al. 2012; Markov et al. 2004; Swinney et al. 1999) reported a unique interferometry technique based on backscatter interferometry (BSI). It employed a simple scalable optical train, which could be used to probe ultra-small volumes and for "on-chip" detection with no modifications to the channel. BSI comprises a laser source, a sample channel, and a photodetector. The laser irradiates the sample located in the channel, the walls of which refract the light multiple times and it is reflected back from the channel in the form of a set of high-contrast interference fringes. The change in the spatial position of the fringe pattern (which arises from interactions between the molecular species in the sample) can be determined by the change in light intensity detected by a photodetector. The magnitude of the change depends on the structural alterations that occur with molecular interactions and the variations in the concentrations of the interacting species. Thus, when LC confined in a rectangular

channel is irradiated by a laser with intensity I_0 at a certain angle, a series of high-contrast fringes results. A change in the orientation of the LC sample 4-cyano-4′-pentylbiphenyl (5CB) (i.e., change in Δn) changes the spatial position of the fringes, causing a change in the intensity (I), defined as

$$I = I_0 \sin^2 \varphi \sin^2\left(\frac{\Gamma}{2}\right) = I_0 \sin^2 \varphi \sin^2\left(\frac{\Delta n}{2}\right) \cdot d \qquad (2)$$

where I_0 and φ are the intensity and angle of the incident laser light, respectively, and d is the distance travelled by the light through the sample.(Dierking 2003)

We designed an LC-based BSI biosensor with glucose as a model analyte. A square glass capillary was filled with 5CB, a nematic LC at room temperature. The LC/aqueous interface was functionalized with a coating of an amphiphilic diblock copolymer of poly(acrylicacid-b-4-cyanobiphenyl-4′-undecylacrylate) (PAA-b-LCP) and immobilized with the enzymes glucose oxidase (GOx) and horseradish peroxidase (HRP) through a covalent linkage to the PAA chains. A change in the intensity of the laser beam focused on the LC/aqueous interface was observed in real time after the aqueous solution was replaced with glucose solution. The detection limit, linear dynamic range, and reproducibility of the biosensor applications using the LC-based BSI setup with glucose solution and human serum were also tested.

2. Materials and Methods

2.1. Materials

Square glass capillaries (0.1 mm wide) were cleaned with piranha solution (***caution***: piranha solution is extremely corrosive and must be handled carefully), subsequently washed with distilled water, and dried under nitrogen. The following substances were used as received: GOx (EC 1.1.3.4) from *Aspergillus niger* as a salt-free lyophilized

powder with a specific activity of >100 units/mg and a molecular weight of 1.6×10^5 g/mol, HRP (EC 1.11.1.7) type VI as a salt-free lyophilized powder with a specific activity of 330 units/mg, *N*-(3-dimethylaminopropyl)-*N*-ethylcarbodiimide hydrochloride (EDC·HCl), and *N*-hydroxysulfosuccinimide sodium salt (NHS) (from Sigma-Aldrich);D(+)glucose, D(+)galactose, ascorbic acid (AA), uric acid (UA), and hemoglobin (Hb)(from Sigma Life Science);trifluoroacetic acid (TFA, 99%), methanol, and dichloromethane (DCM)(from Aldrich);5CB [100%, Tokyo Chemical Industry (TCI)]; and NaCl and octadecyltrichlorosilane (OTS) (from Sigma Aldrich). The amphiphilic block copolymer PAA-b-LCP was synthesized using the same method reported in our previous study(Lee et al. 2010)and had a molecular weight of PAA (11K)-b-LCP (5K) with M_w/M_n= 1.14.

2.2. Instrumentation of the LC-based BSI

The BSI setup included a He–Ne laser (30 mW, 25-LHP-991-230, Melles Griot, Carlsbad, CA, USA), photodetector (New Focus 2001, Newport Corporation, Irvine, CA, USA), data acquisition (DAQ) board (NIcDAQ-9172, National Instruments), voltage controller (NI9205, National Instruments), and mirror (National Instruments) as shown in Figure 1a. A He–Ne laser beam (λ = 632.8 nm, diameter = 100 μm) was diverted by a mirror 3 cm below the laser source and at an approximately 45° angle with respect to the incident beam. The mirror focused the beam onto the 5CB near the 5CB/aqueous interface in the OTS-coated square capillary. The square glass capillary was filled with 5CB upto 1 mm by dipping one end of the capillary into the 5CB. The dipped side of the capillary was then sealed with glue (Araldite® Rapid, Huntsman Advanced Materials, Everberg, Belgium). A round capillary was inserted into the open end of the square

capillary, and the two capillaries were connected by a T-connector, as shown in Figure 1b. Solutions were presented to the LC/aqueous interface via the round capillary, and they exited at one end of the T-connector (inset Figure 1b shows the dimensions of T-connector) represented by the arrows. The resulting backscattered interference fringe pattern was focused onto the photodetector, which consisted of a small-area photodiode (0.9 mm diameter) and was located 10 cm from the sample (Figure 1a). The photodiode was aligned with the edge of a single backscattered fringe (the third fringe to the right of the centroid; the need for fringe selection is discussed in a later section). We measured a variation in intensity when there was a shift in the position of the backscattered fringe due to a change in the orientation of the 5CB within the capillary (Figure 1c). Spatial movement of the backscattered fringe produced a change in the total light intensity that struck the active area of the photodetector and a subsequent change in the output voltage of the detector.

2.3. Functionalization of PAA-b-LCP and GOx:HRP

Silicon tubing attached to a syringe pump (KD Scientific, KDS 100 series, USA) placed the PAA-b-LCP aqueous solution (1 mg/mL) on the 5CB surface in the square capillary at a flow rate of 0.02 mL/min. After about 2 h, the solution formed a self-assembled monolayer at the 5CB/aqueous interface. The LCP block was adsorbed into the 5CB and the PAA chains formed a brush at the interface. GOx and HRP were both immobilized to the PAA-b-LCP–coated 5CB ($5CB_{PAA}$) using a slight modification of a method reported elsewhere.(Steffens et al. 2002) Briefly, the PAA chains were activated with 0.4 M EDC·HCl and 0.1 M NHS solution for 1 h, after which 1 mL of the GOx:HRP (31.25:12.5 μM) mixture solution was passed through the flow capillary cell and held at

room temperature for 4 h. The sensor cell was denoted $5CB_{PAA\text{-}GOx:HRP}$. The polarized optical microscope (POM) of the sensor cell were captured using POM (ANA-006, Leica Microsystems, Wetzlar, Germany) images under crossed polarizers were captured with a CCD camera (STC-TC83USB, Samwon Electronics, Seoul, Korea). The presence of PAA and GOx at the 5CB/aqueous interface was confirmed by the covalent linking of the fluorescent dye rhodamin 6G with the PAA chains via a water-soluble carbodiimide reaction and GOx labeled with rhodamin 6G ($GOx_{rhodamin6G}$) using a fluorescence microscope (Eclipse, E600POL, Nikon Instruments, Melville, NY, USA). The sensor cell was then placed on a black non-reflective sheet, and the BSI data for all samples were recorded 1 min after the introduction of solutions. Three measurements were made and the error bars represent the standard deviation (SD).

2.4. Labeling of GOx

GOx was labeled with rhodamin 6G using a slightly modified previously reported method.(Steffens et al. 2002) Briefly, chemical coupling agents EDC·HCl and NHS solution were added to a GOx solution (20 µM). The mixture was kept at 4 °C for 1 h to activate the carboxylic acid groups in GOx. Subsequently, 1 mg of rhodamin 6G was added and the mixture was stirred for 4 h at room temperature. A saturated aqueous ammonium sulfate solution (0.5g/mL) was added dropwise to the mixture. The rhodamin 6G-labeled GOx ($GOx_{rhodamin6G}$) was precipitated out and centrifuged twice at 5000 rpm for 20 min. The supernatant was then removed by filtration and the sediment powder was dried under vacuum to yield $GOx_{rhdodamin6G}$. The success of the labeling was confirmed by a UV-visible spectrum (Figure SI-3).

2.5. Automated real Time Data processing and acquisition:

A program that performs the necessary calculations in real time was designed, implemented, and evaluated. The code for a simple graphical interface in the LC-based BSI was developed using LabVIEW™ (LV) 2012 (National Instruments, Austin, TX, USA). Figure SI-1 shows the block diagram and the front panel of the program. To evaluate the functionality of the program, glycerol samples at different glycerol concentrations were introduced into the square capillary to produce a known change in laser intensity (Figure SI-2).

2.6. Biosensor evaluation procedure

The practical evaluation of the LC-based BSI is carried out using human serum. The level of glucose in human serum is measured using high performance liquid chromatography (HPLC). The HPLC analysis was carried out using HPLC instrument (Waters Co. Model 600E) with column (Sugar-Pak I column (6.5×300mm)) and refractive index detector (RI, Model 410). Ca-EDTA buffer (50mg Ca-EDTA/1L dH2O) was used for the mobile phase with a flow rate of 0.5 mL/min at 90°C in the column.

3. Results and Discussion

3.1. Verification of LC orientation in a square capillary

To determine whether the LC-based BSI can detect the change in LC orientation we tested aqueous solutions (10 mg/mL) of SDS ($5CB_{SDS}$) and PVA ($5CB_{PVA}$), which cause homeotropic and planar orientations at the LC/aqueous interface, respectively. The $5CB_{SDS}$ exhibited a dark image and the $5CB_{PVA}$ exhibited a bright image at the LC/aqueous interface when observed under a POM with cross polarizers (Figures 2a and b). Earlier studies reported that an NLC (e.g., 5CB)with SDS had homeotropic and radial

configurations (perpendicular to the surface) and an NLC with PVA had planar and bipolar configurations (parallel to the surface) in flat and spherical geometries, respectively (Dierking 2003). When $5CB_{SDS}$ is in the OTS-coated capillary, the 5CB molecules are aligned perpendicular to the surfaces, giving rise to dark configuration at the LC/water and LC/capillary wall boundaries under cross polarizers. When $5CB_{PVA}$ is in the OTS-coated capillary, the 5CB molecules are aligned tilted with respect to cross polarizers, giving rise bright configuration at the LC/water and LC/capillary wall boundaries. A schematic of the 5CB in a square capillary under cross polarizers is depicted in Figure 2c, in which the dashed and solid lines represent the capillary wall and the 5CB, respectively. The boundary (gray color) is tilted because the square capillary is parallel on the sample stage of the POM. When $5CB_{SDS}$ and $5CB_{PVA}$were in the capillary, the BSI intensities were recorded at the third fringe (choice of this fringe is discussed later), with the baseline intensity (I =0 V) at the 5CB/air interface, as shown in Figure 2d. The saturated intensities obtained when $5CB_{SDS}$ and $5CB_{PVA}$were in the capillary were 2.70 and 5.12 V, respectively, indicating that the LC-based BSI can quantitatively measure change in the orientation of LCs.

Figures 3a and b are POM images (under crossed polarizers) of $5CB_{PAA}$ and $5CB_{PAA\text{-}GOx:HRP}$ exhibiting bright configuration in the capillary. To confirm the presence of PAA chains at the 5CB/aqueous interface, rhodamin 6G-labeled PAA chains were used to locate the PAA chains. The uniformly distributed green color only at the LC/aqueous interface in the fluorescent microscopy image of $5CB_{PAA\text{-}rhodamine6G}$ in the capillary (Figure 3c) confirms the monolayer formation of PAA-b-LCP at the interface. A similar uniformly distributed green color (Figure 3d) was observed at the 5CB/aqueous

interface with $5CB_{PAA\text{-}GOx\text{-}rhodamine6G}$ in the capillary. Next, $5CB_{PAA\text{-}GOx:HRP}$ was tested to detect glucose. A change in orientation of 5CB from bright to dark configuration was observed (Figure 3e) when the aqueous medium in the capillary was replaced with a 20 mM glucose solution (100μL). This change in 5CB orientation may have been caused by the GOx-catalyzed oxidation of glucose and the subsequent reduction of H_2O_2 by HRP.(Sassolas et al. 2012)To confirm the role of the enzymes in $5CB_{PAA\text{-}GOx:HRP}$, a 20 mM galactose (stereoisomer of glucose) solution replaced the glucose solution. The initial bright configuration remained, indicating that the change from bright to dark configuration was due to enzymatic reaction. Thus, $5CB_{PAA\text{-}GOx:HRP}$ in the capillary can be a glucose biosensor in the LC-based BSI.

3.2. Selection of the fringe

In our LC-based BSI, a series of backscattered fringes are produced when the laser beam is incident on $5CB_{PAA\text{-}GOx:HRP}$ in the square capillary. Therefore, it is important to demonstrate which fringe should be used for the acquisition of data. Fringes are separate from the centroid, which is larger and can be easily distinguished from other fringes. The centroid may be produced by reflection from the surface of the capillary. Figure 4 presents saturated intensity vs. different concentration of glucose (C_0) curves using the third, fourth, fifth, sixth, and tenth fringes for data acquisition. The slopes 0.3746, 0.3774, 0.3793, and 0.3492 for the third, fourth, fifth, and sixth fringes, respectively, are almost identical within the experimental error range. The slope for the tenth fringe is 0.2938. These data suggest that the use of a particular backscatter fringe is not necessary, although data that are more accurate are obtained using the third to sixth fringes. In this study the data is obtained from third fringe for all experiments unless otherwise specified.

3.3. Glucose detection with LC-based BSI:

The photodiode detector was positioned on the edge of a backscattered fringe [I = 0 V; Figure 5a(i)] from $5CB_{PAA\text{-}GOx:HRP}$ in the square capillary without glucose. There was an increase in I from 0 to 3.58 V [Figure 5a(ii)] after replacing the aqueous medium with a 20 mM glucose solution. In a bienzyme GOx:HRP system the immobilized HRP^{+3} reduces the H_2O_2 to hydroxyl ions (OH^-) and oxidizes itself to HRP^{+5} as summarized in Scheme 1. The OH^- take the available protons (H^+) in the system and produce water. Then, HRP^{5+} reverts to HRP^{+3}owing to the dual role of H_2O_2 as an oxidant in the formation of HRP^{+5} and a typical one-electron donor (reductant for peroxidase), which yields a hydroperoxyl radical ($HO_2^{\bullet}$) and a superoxide ion radical ($O_2^{\bullet-}$).(Hernández-Ruiz et al. 2001) The $O_2^{\bullet-}$ is a highly reactive intermediate and can readily react with H^+ to form $HO_2^{\bullet}$. The two $HO_2^{\bullet}$ form H_2O_2 and O_2. Next, the H_2O_2 decomposes to OH^- in the presence of a reducing agent (e.g., HRP) and the reaction continues as more H_2O_2 and H^+ become available.(Praus et al. 2012) Thus, the OH^-generated by the HRP-catalyzed reduction of H_2O_2requires H^+, leading to the deprotonation of the carboxylic acid (COOH) groups in the PAA chains and generating a high density of negative charges. These negative charges alter the 5CB configuration, as shown in Figure 4b.High charge density causes perpendicular orientation that leads to homeotropic (or radial) configuration. For example, the 5CB in a transmission electron microscopy (TEM) grid was functionalized with block copolymers consisting of polyelectrolytes (PEs), such as quaternized poly(4-vinylpyridine) (QP4VP),(Omer and Park 2014) polystyrenesulfonate (PSS),(Omer et al. 2014a) and poly(dimethylaminoethylmethacrylate) (PDMAEA).(Omer et al. 2014b)When 5CB was coated with QP4VP (a strong cationic

PE) and PSS (a strong anionic PE), orientation was homeotropic regardless of pH. However, the orientation was pH-dependent when 5CB was coated with PAA (a weak anionic PE) and PDMAEA (a weak cationic PE) because of deprotonation and protonation of the pendant group above and below their pK_a values, respectively. To confirm that this change in intensity was due to the glucose catalyzed by reaction of the GOx:HRP cascade, $5CB_{PAA\text{-}GOx}$ (without immobilized HRP) was subjected to a 20 mM glucose solutionand there was no increase in *I* [Figure 5a(iii)]. Similarly, when $5CB_{PAA\text{-}HRP}$ (without immobilized GOx) was subjected to the same solution, *I* did not change, but when a 10 mM H_2O_2 solution was used, *I* increased to 3.83 V [Figure 5a(iv)]. When 10 mM H_2O_2 solution was injected into enzyme-free $5CB_{PAA}$, *I* remained 0 V [Figure 5a(v)]. These results suggest that the glucose catalyzed by GOx:HRP altered the 5CB orientation at the 5CB/aqueous interface (Figure 5b), leading to a change in intensity in the BSI. The orientation of 5CB may be controlled by the charge density of the PAA chains at the 5CB/aqueous interface. Dong et al.(Dong et al. 2009) studied the dissociation behavior of PAA brushes at different pH. They found that the deprotonation of the COOH groups to COO^- in the brush was more difficult than that in the bulk PAA chains, resulting in a higher pKa value (6.5–6.6) than that for the free-moving PAA chains (pKa 4.7). The terminal COOH groups start to deprotonate at pH 6.5–6.6, while the deprotonation of the bulk COOH group increases as pH increases beyond 6.6, achieving a complete conversion of COOH to COO^- at pH=9. Yang et al.(Yang et al. 2015) found that the 5CB droplets were functionalized by ionic surfactants followed by alternate coats of the oppositely charged PEs PSS and QP4VP. The reversible change in configuration from radial to bipolar by the adsorption of the oppositely charged PEs occurred because of a

change in the net electric field on the surface of the droplets. Thus, these findings confirm that the change in *I* in BSI was due to the glucose-catalyzed reaction at the LC/aqueous interface.

Figure 6a shows the LC-based BSI spectra of intensity with respect to time for different concentrations of glucose (C_0 = 0.02–10 mM) recorded over 2 min. The intensity increased with time and reached a saturation level after ~1min. Figure 6b shows that the saturated intensity linearly increased as C_0 increased up to C_0=9 mM and then leveled off, indicating that the linear dynamic detection range was 0.02–9 mM. A slight change in intensity was found when C_0<0.02 mM; however, the cause of this change was not clear but may have been due to the noise signal of the BSI. The instrument detection limit (IDL) (i.e., the analyte concentration needed to produce intensity greater than three times the standard deviation of the noise level) is important because most analytical instruments produce a noise signal without analyte present. The IDL for the LC-based BSI was 0.008 mM, which was calculated using ten blanks with I = 0.011 ± 0.0027. Thus, LC-based BSI enables the detection of a small amount of glucose in solution and has a large linear dynamic detection range compared to texture-reading methods. For example, a TEM grid filled with 5CB was used for glucose detection and its linear range measured from Δn was 0.05–2 mM. Another study reported a range of 0.02–1 mM with GOx:HRP at the 5CB/aqueous interface in the TEM grid cell.(Khan and Park 2015a) These small linear dynamic ranges were due to difficulty in measuring the small difference in Δn, where the change in texture color was very small and could not be differentiated by the naked eye using POM. However, because the LC-based BSI can

monitor small changes in the orientation of 5CB resulting from C_0, it could be used for quantitative analysis with biosensors.

3.4. Interference from other analytes and practical evaluation

The LC-based BSI was tested for the interference caused by common interfering species present in blood. $5CB_{PAA\text{-}GOx:HRP}$ was exposed to 0.1 mM AA, 0.3 mM UA, 0.1 wt% Hb, 10 mM cholesterol, 0.1 wt% BSA, 0.1 M NaCl, and 0.1 M $FeCl_3$. The AA and UA concentrations used are the maximum concentrations possible for those acids in blood. Similarly, red blood cells contain a large amount of Hb, which may interfere with glucose. However, there was no change in the saturated intensity with the presence of these analytes, as shown in Figure 7. We tested the performance of the LC-based BSI in detecting glucose in pure and diluted (100 µl/mL) human serum. Human serum contains cholesterol, glucose, sodium, iron, proteins, endotoxin, and triglyceride. The intensities for pure and diluted serum were 1.83 and 0.17 V, respectively, indicating that the change in intensity was due to the presence of glucose and corresponded to the glucose concentration of ~5.5 mM from the calibration curve in Figure 6b. In order to check the exact amount of glucose in the serum, a standard curve C_0 = 2 to 11 mM was obtained by using a HPLC technique (Figure SI 4). The glucose content in serum is 5.32 mM from HPLC, comparable to that obtained from LC-based BSI. Thus, the $5CB_{PAA\text{-}GOx:HRP}$ provides enough specificity for glucose detection and quantitative measurement.

3.5. Reproducibility

The reproducibility of the LC-based BSI data was characterized by alternately exposing $5CB_{PAA\text{-}GOx:HRP}$ to a glucose solution and PBS buffer (pH6). Figure 8 shows the intensity of $5CB_{PAA\text{-}GOx:HRP}$ in the capillary when the LCs were sequentially exposed to 1mM

glucose solution, PBS buffer, 3mM glucose solution, and PBS buffer in cycles. We used different concentrations of glucose solution to check whether the sensitivity with respect to glucose concentration was maintained after washing with PBS. The intensity for each cycle was 0.012±0.0015 after washing with PBS and increased to 0.29 ± 0.002 and 1.14 ± 0.0015 after exposure to the 1 and 3mM glucose solutions, respectively. These results show that LC-based BSI data are reproducible and that the LC-based BSI can be used for multiple detections, even at different glucose concentrations.

4. Conclusion

Quantitative detection of a glucose biosensor was successfully demonstrated using a LC-based BSI. The 5CB LC confined in an OTS-coated square capillary was functionalized by a coating of PAA-b-LCP at the LC/aqueous interface and subsequently immobilized by GOx:HRP for glucose detection. The new LC-based BSI has high sensitivity (0.02 mM), instrument detection limit (0.008 mM), linear dynamic range (0.02-9 mM), selectivity, ease of detection, reproducibility, and ability of quantitative measurement at LC /aqueous interface. The LC-based BSI offers simple and real time quantitative detection at LC/aqueous interface compared to earlier reports those utilized texture reading or birefringence measurement. Thus, this technology can be expanded to other LC-based biosensors using antibodies, aptamers, and other enzymes.

Acknowledgment

This work was supported by the National Research Foundation of Korea (NRF-2011-0020264 and NRF-2014R1A2A1A11050451).

References

Bornhop, D.J., Latham, J.C., Kussrow, A., Markov, D.A., Jones, R.D., Sørensen, H.S., 2007. Free-Solution, Label-Free Molecular Interactions Studied by Back-Scattering Interferometry. Science 317(5845), 1732-1736.

Brake, J.M., Daschner, M.K., Luk, Y.Y., Abbott, N.L., 2003. Biomolecular Interactions at Phospholipid-Decorated Surfaces of Liquid Crystals. Science 302, 2094-2097.

Carlton, R.J., Gupta, J.K., Swift, C.L., Abbott, N.L., 2012a. Influence of simple electrolytes on the orientational ordering of thermotropic liquid crystals at aqueous interfaces. Langmuir 28(1), 31-36.

Carlton, R.J., Ma, C.D., Gupta, J.K., Abbott, N.L., 2012b. Influence of Specific Anions on the Orientational Ordering of Thermotropic Liquid Crystals at Aqueous Interfaces. Langmuir 28(35), 12796-12805.

Chen, X., Zhang, X.-E., Chai, Y.-Q., Hu, W.-P., Zhang, Z.-P., Zhang, X.-M., Cass, A.E.G., 1998. DNA optical sensor: a rapid method for the detection of DNA hybridization. Biosensors and Bioelectronics 13(3–4), 451-458.

Deng, J., Liang, W., Fang, J., 2016. Liquid Crystal Droplet-Embedded Biopolymer Hydrogel Sheets for Biosensor Applications. ACS Applied Materials & Interfaces 8(6), 3928-3932.

Dierking, I., 2003. Textures of Liquid Crystals. Wiley, Weinheim.

Dong, R., Lindau, M., Ober, C.K., 2009. Dissociation Behavior of Weak Polyelectrolyte Brushes on a Planar Surface. Langmuir 25(8), 4774-4779.

Gupta, V.K., Skaife, J.J., Dubrovsky, T.B., Abbott, N.L., 1998. Optical Amplification of Ligand-Receptor Binding Using Liquid Crystals. Science 279, 2077-2080.

Haddad, G.L., Young, S.C., Heindel, N.D., Bornhop, D.J., Flowers, R.A., 2012. Back-Scattering Interferometry: An Ultrasensitive Method for the Unperturbed Detection of Acetylcholinesterase–Inhibitor Interactions. Angewandte Chemie International Edition 51(44), 11126-11130.

Hariharan, P., 2007. Basics of Interferometery, 2 ed. Elsevier, California

Hernández-Ruiz, J., Arnao, M.B., Hiner, A.N., García-Cánovas, F., Acosta, M., 2001. Catalase-like activity of horseradish peroxidase: relationship to enzyme inactivation by H2O2. Biochemical Journal 354(Pt 1), 107-114.

Hsu, P., Poulin, P., Weitz, D.A., 1998. Rotational Diffusion of Monodisperse Liquid Crystal Droplets. Journal of Colloid and Interface Science 200(1), 182-184.

Khan, M., Khan, A.R., Shin, J.-H., Park, S.-Y., 2016. A liquid-crystal-based DNA biosensor for pathogen detection. Scientific Reports 6, 22676.

Khan, M., Kim, Y., Lee, J.H., Kang, I.-K., Park, S.-Y., 2014. Real-time liquid crystal-based biosensor for urea detection. Analytical Methods 6(15), 5753-5759.

Khan, M., Park, S.-Y., 2014a. General Liquid-crystal droplets produced by microfluidics for urea detection. Sensors and Actuators B: Chemical 202(0), 516-522.

Khan, M., Park, S.-Y., 2014b. Liquid Crystal-Based Proton Sensitive Glucose Biosensor. Analytical Chemistry 86(3), 1493-1501.

Khan, M., Park, S.-Y., 2015a. Glucose biosensor based on GOx/HRP bienzyme at liquid–crystal/aqueous interface. Journal of Colloid and Interface Science 457, 281-288.
Khan, M., Park, S.-Y., 2015b. Liquid crystal-based glucose biosensor functionalized with mixed PAA and QP4VP brushes. Biosensors and Bioelectronics 68, 404-412.
Kim, J., Khan, M., Park, S.-Y., 2013. Glucose Sensor using Liquid-Crystal Droplets Made by Microfluidics. ACS Applied Materials & Interfaces 5(24), 13135-13139.
Lee, D.Y., Seo, J.M., Khan, W., Kornfield, J.A., Kurjib, Z., Park, S.Y., 2010. pH-responsive aqueous/LC interfaces using SGLCP-b-polyacrylic acid block copolymers. Soft Matter 6, 1964-1970.
Liao, S., Ding, H., Wu, Y., Wu, Z., Shen, G., Yu, R., 2016. Label-free liquid crystal biosensor for L-histidine: A DNAzyme-based platform for small molecule assay. Biosensors and Bioelectronics 79, 650-655.
Lin, I.H., Miller, D.S., Bertics, P.J., Murphy, C.J., de Pablo, J.J., Abbott, N.L., 2011. Endotoxin-Induced Structural Transformations in Liquid Crystalline Droplets. Science 332(6035), 1297-1300.
Loudet, J.C., Hanusse, P., Poulin, P., 2004. Stokes Drag on a Sphere in a Nematic Liquid Crystal. Science 306(5701), 1525-1525.
Malik, P., Raina, K.K., 2004. Droplet orientation and optical properties of polymer dispersed liquid crystal composite films. Optical Materials 27(3), 613-617.
Markov, D.A., Swinney, K., Bornhop, D.J., 2004. Label-Free Molecular Interaction Determinations with Nanoscale Interferometry. Journal of the American Chemical Society 126(50), 16659-16664.
Munir, S., Park, S.-Y., 2015. The development of a cholesterol biosensor using a liquid crystal/aqueous interface in a SDS-included β-cyclodextrin aqueous solution. Analytica Chimica Acta 893, 101-107.
Munir, S., Park, S.-Y., 2016. Liquid crystal-Based DNA biosensor for myricetin detection. Sensors and Actuators B: Chemical 233, 559-565.
Niu, X., Luo, D., Chen, R., Wang, F., Sun, X., Dai, H., 2016. Optical biosensor based on liquid crystal droplets for detection of cholic acid. Optics Communications 381, 286-291.
Omer, M., Islam, M., Khan, M., Kim, Y., Lee, J., Kang, I.-K., Park, S.-Y., 2014a. Liquid crystal-based biosensors using a strong polyelectrolyte-containing block copolymer, poly(4-cyanobiphenyl-4′-oxyundecylacrylate)-b-poly(sodium styrene sulfonate). Macromol. Res. 22(8), 888-894.
Omer, M., Khan, M., Kim, Y.K., Lee, J.H., Kang, I.-K., Park, S.-Y., 2014b. Biosensor utilizing a liquid crystal/water interface functionalized with poly(4-cyanobiphenyl-4′-oxyundecylacrylate-b-((2-dimethyl amino) ethyl methacrylate)). Colloids and Surfaces B: Biointerfaces 121(0), 400-408.
Omer, M., Park, S.-Y., 2014. Preparation of QP4VP-b-LCP liquid crystal block copolymer and its application as a biosensor. Anal Bioanal Chem, 1-10.
Patel, J.S., Yokoyama, H., 1993. Continuous anchoring transition in liquid crystals. Nature 362(6420), 525-527.
Praus, P., Matys, J., Kozák, O., 2012. Photocatalytic decomposition of phenol by nanocomposite of ZnS nanoparticles and montmorillonite. Journal of the Brazilian Chemical Society 23, 1900-1906.
Ready, J.F., Industrial Applications of Lasers, 2 ed. Academic Press, Chestnut Hill MA USA.
Sassolas, A., Blum, L.J., Leca-Bouvier, B.D., 2012. Immobilization strategies to develop enzymatic biosensors. Biotechnology Advances 30(3), 489-511.
Steffens, G.C.M., Nothdurft, L., Buse, G., Thissen, H., ocker, H.H., Klee, D., 2002. High density binding of proteins and peptides to poly(d,l-lactide) grafted with polyacrylic acid. Biomaterials 23, 3523-3531.
Swinney, K., Markov, D., Hankins, J., Bornhop, D.J., 1999. Micro-interferometric backscatter detection using a diode laser. Analytica Chimica Acta 400(1–3), 265-280.
Symietz, C., Schneider, M., Brezesinski, G., Möhwald, H., 2004. DNA Alignment at Cationic Lipid Monolayers at the Air/Water Interface. Macromolecules 37(10), 3865-3873.
Tan, H., Yang, S., Shen, G., Yu, R., Wu, Z., 2010. Signal-Enhanced Liquid-Crystal DNA Biosensors Based on Enzymatic Metal Deposition. Angewandte Chemie International Edition 49(46), 8608-8611.

Tyagi, M., Chandran, A., Joshi, T., Prakash, J., Agrawal, V.V., Biradar, A.M., 2014. Self assembled monolayer based liquid crystal biosensor for free cholesterol detection. Applied Physics Letters 104(15), 154104.
Yang, L., Khan, M., Park, S.-Y., 2015. Liquid crystal droplets functionalized with charged surfactant and polyelectrolyte for non-specific protein detection. RSC Advances 5(118), 97264-97271.
Zhao, D., Peng, Y., Xu, L., Zhou, W., Wang, Q., Guo, L., 2015. Liquid-Crystal Biosensor Based on Nickel-Nanosphere-Induced Homeotropic Alignment for the Amplified Detection of Thrombin. ACS Applied Materials & Interfaces 7(42), 23418-23422.
Zhao, Y., Mahaja, N., Fang, J., 2006. Self-Assembled Cylindrical Lipid Tubules with a Birefringent Core. Small 2(3), 364-367.

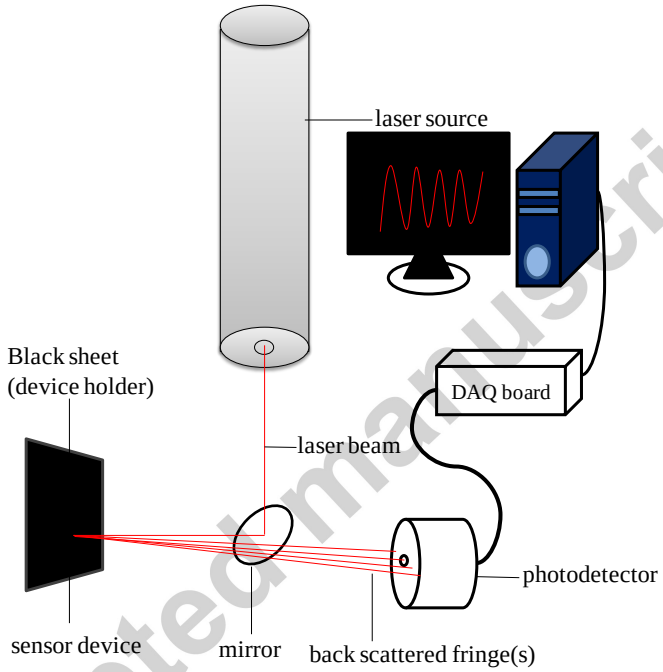

(a)

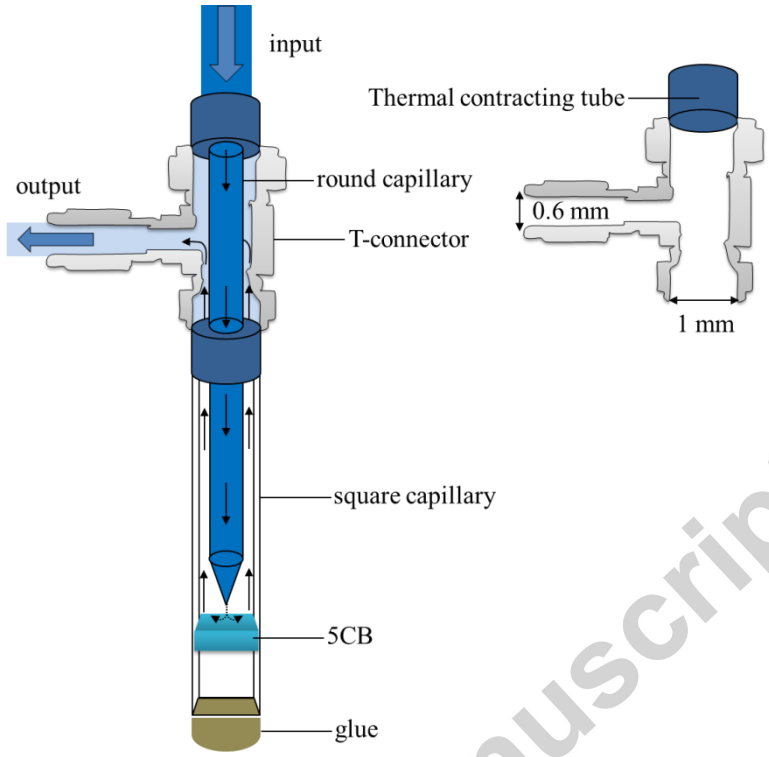

(b)

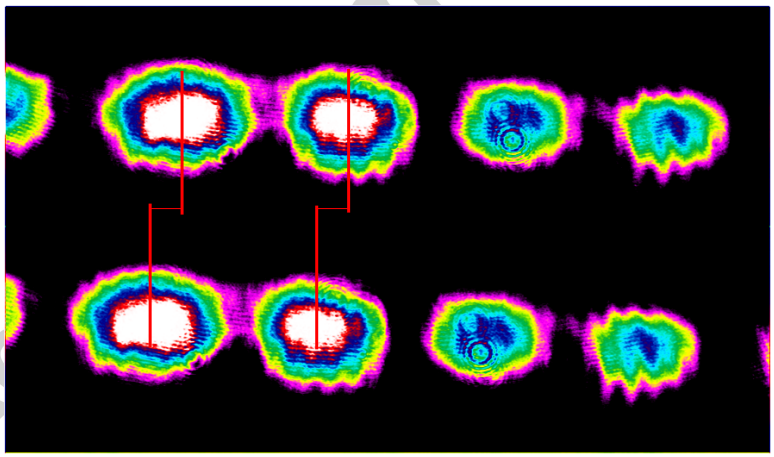

(c)

Figure 1. Schematic representation of (a) BSI setup, and (b) sensor cell with the dimensions of T-connector, and (c) false-color reconstruction of the patterns of the backscattered fringes from 5CB confined in a square capillary. The change in fringe position corresponds to the change of Δn resulting from the change in the orientation of 5CB. The arrows in (b) show how the solution(s) flow in the sensor cell.

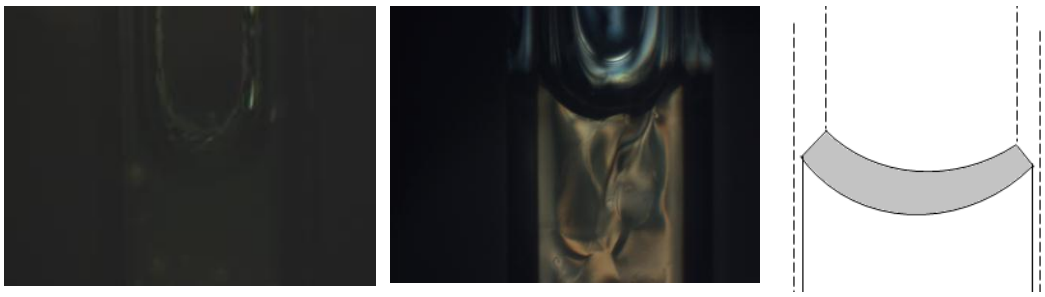

(a) (b) (c)

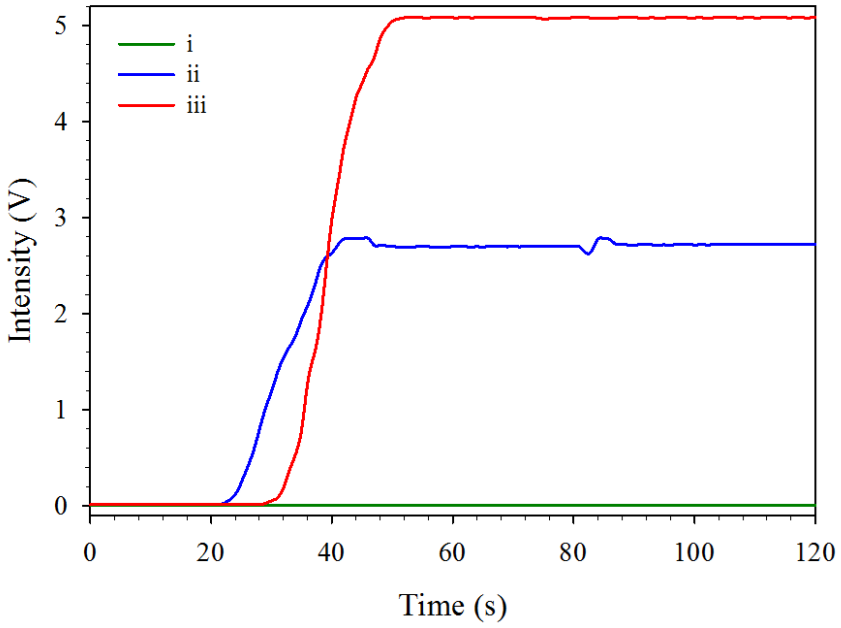

(d)

Figure 2. POM images of 5CB in the square capillary with 10 mg/mL aqueous solutions of (a) SDS and (b) PVA. (c) Schematic of 5CB in a square capillary under cross polarizers, where the dashed and solid lines represent the capillary wall and 5CB, respectively. (d) LC-based BSI spectra of (i) 5CB/air interface (padded at I = 0 V), (ii) $5CB_{SDS}$, and (iii) $5CB_{PVA}$ in the square capillary.

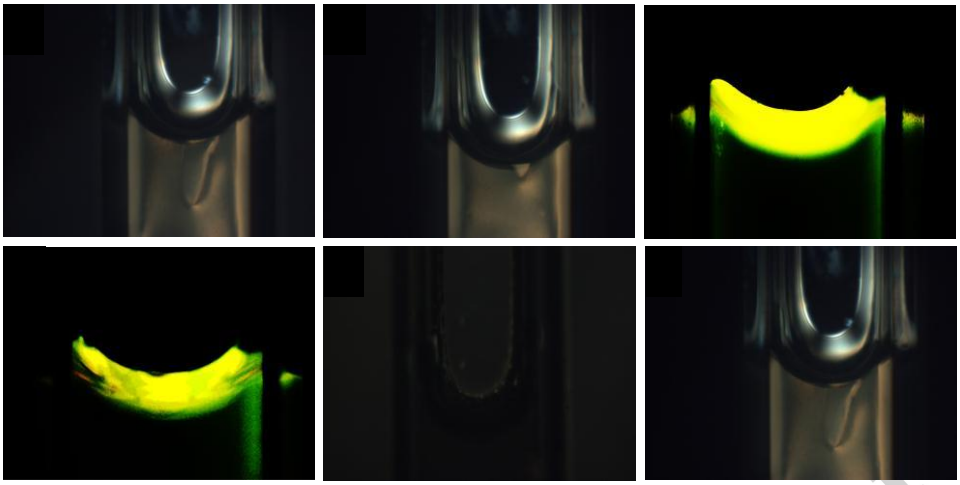

Figure 3. POM images of (a) $5CB_{PAA}$ and (b) $5CB_{PAA:GOx:HRP}$ in the capillary. Fluorescence images of (c) $5CB_{PAA\text{-}rhodamin6G}$ and (d) $5CB_{PAA\text{-}GOx\text{-}rhodamin6G}$ in the capillary. POM images of $5CB_{PAA\text{-}GOx:HRP}$ in the capillary with 20 mM aqueous solutions of (e) glucose and (f) galactose.

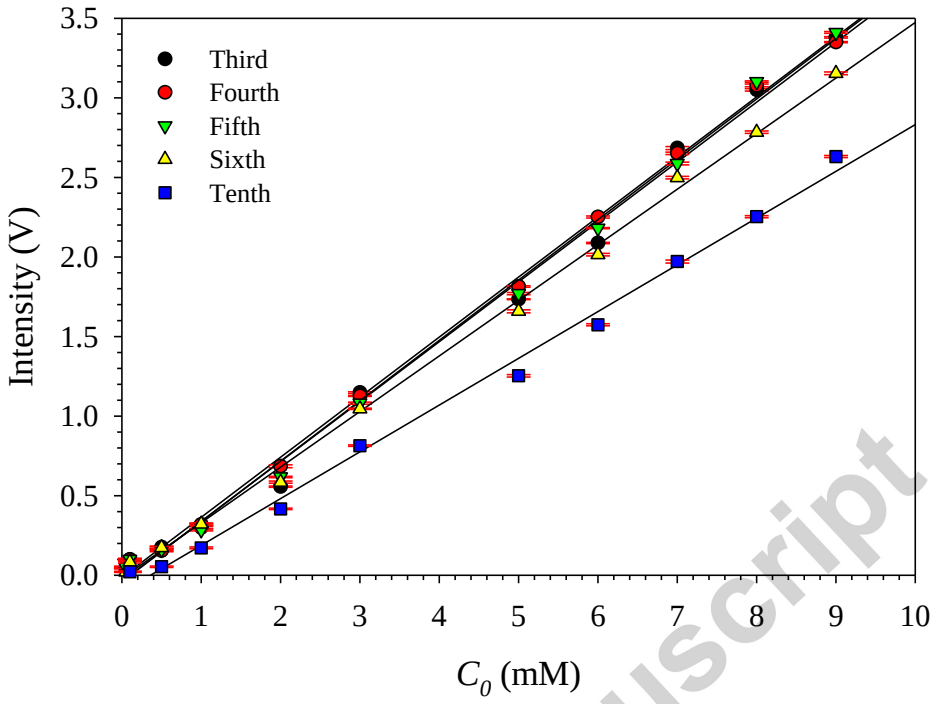

Figure 4. Intensity vs. C_0 (0.02–9 mM), with data obtained using various fringes to the right of the centroid. Error bars represent standard deviation.

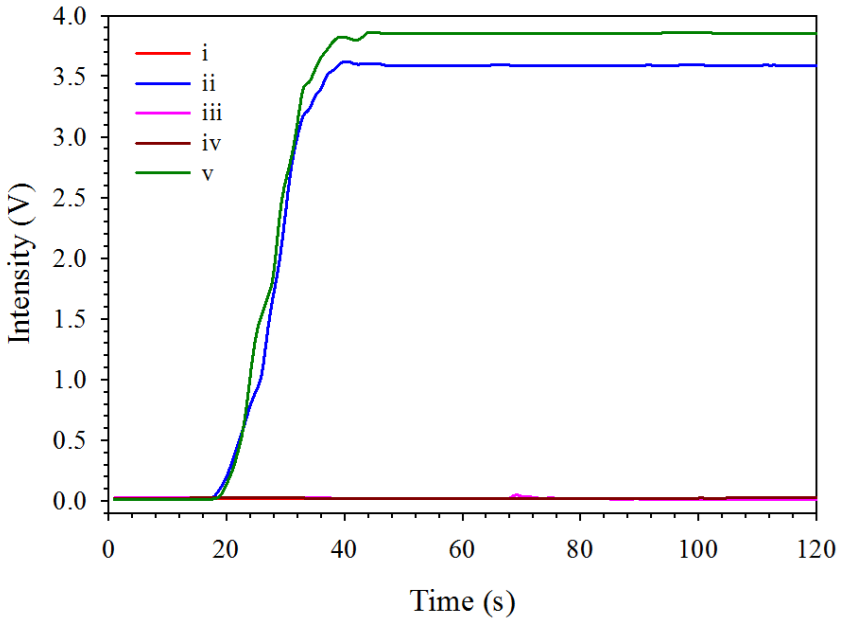

(a)

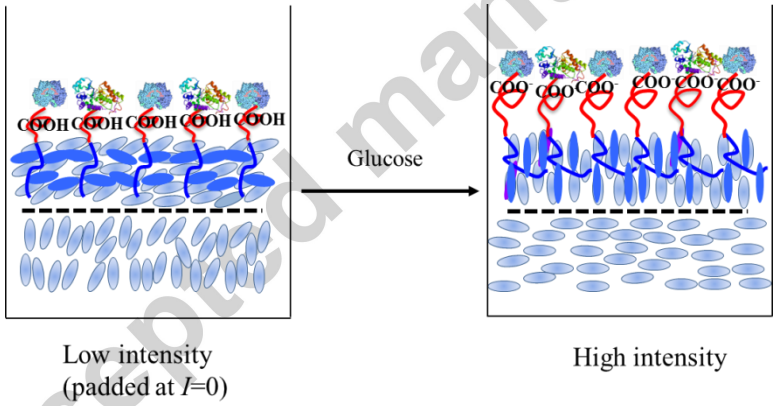

(b)

Figure 5. (a) LC-based BSI spectra of the backscattered fringes of (i) $5CB_{PAA\text{-}GOx:HRP}$ in the capillary aligned at I = 0 V, (ii) $5CB_{PAA\text{-}GOx:HRP}$ and (iii) $5CB_{PAA\text{-}GOx}$ in the capillary with a 20 mM glucose solution, and $5CB_{PAA\text{-}HRP}$ in the capillary with (iv) 20 mM glucose and (v) 10 mM H_2O_2 solutions. (b) Schematic of $5CB_{PAA\text{-}GOx:HPR}$ (left) before and (right) after exposure to a glucose solution.

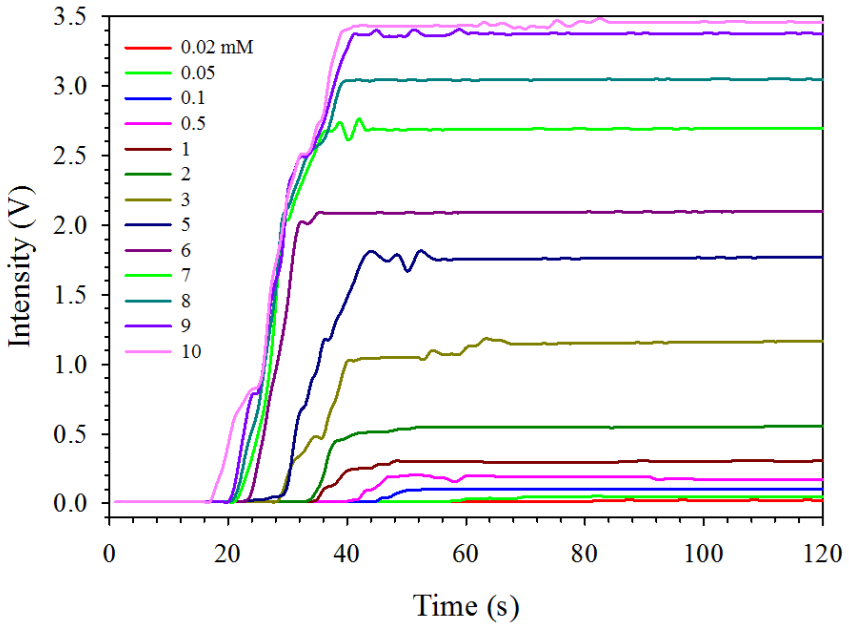

(a)

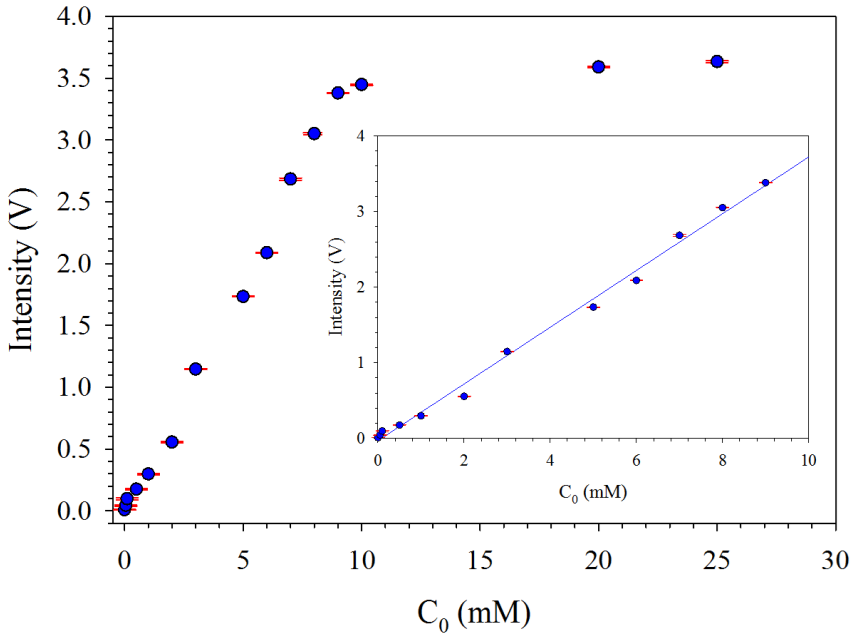

(b)

Figure 6. (a) LC-based BSI spectra for glucose at different concentrations (C_0). (b) Saturated intensity as a function of C_0; the inset shows the intensity calibration curve for C_0 = 0.02–9 mM. Error bars in the graph are smaller than the data points.

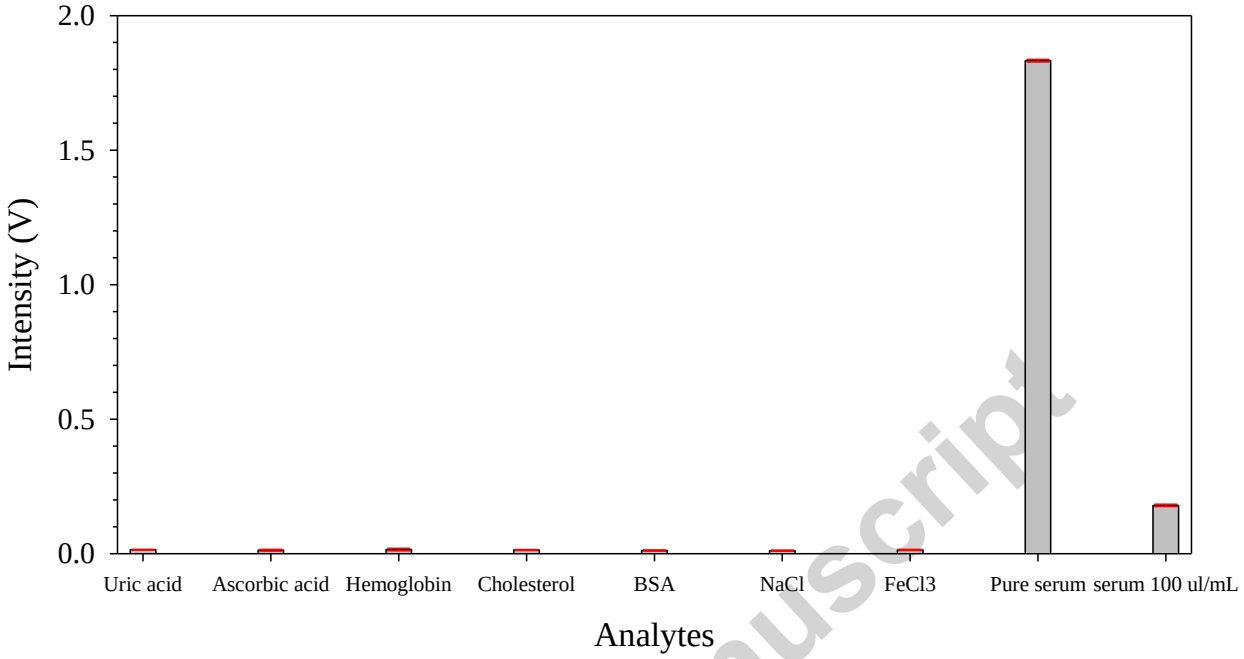

Figure 7. Intensity of the LC-based BSI for various electroactive species present in blood and human serum. Error bars represent standard deviation.

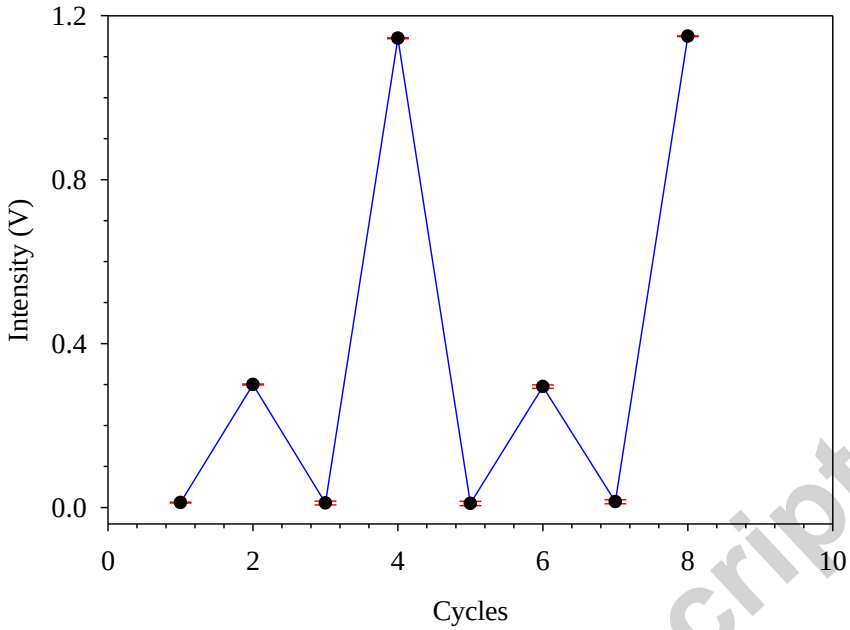

Figure 8. LC-based BSI intensity when the LCs are sequentially exposed to 1 mM glucose solution, PBS buffer, 3 mM glucose solution, and PBS buffer. Error bars represent standard deviation.

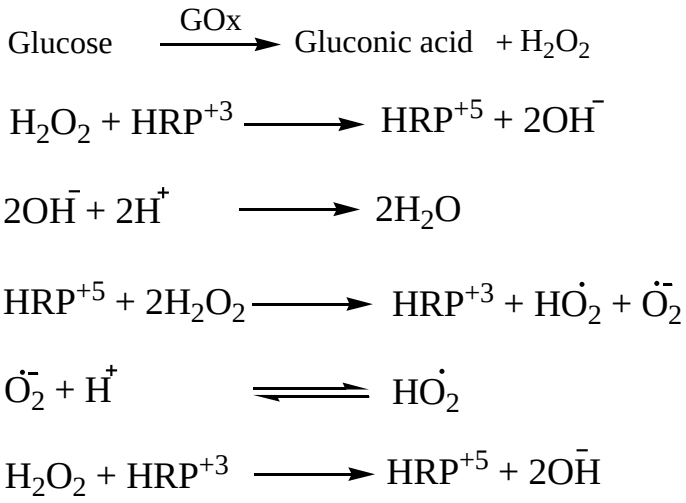

Scheme 1. GOx catalyzed-oxidation of glucose followed by HRP catalyzed-reduction of H_2O_2 in the presence of available H^+.

Highlights

- A new technology that enabled quantitative detection at liquid crystal/aqueous interface was developed.
- This method uses backscattering interferometry (BSI) and liquid crystal (LC) confined in a square capillary.
- Glucose was used as a model analyte.
- The change in the spatial position of the laser fringes altered the output voltage of the photodetector.
- The change in the intensity at the photodetector allowed the detection of the analyte.